# High Performance 84-Pulse Driver for Speed Control of Permanent Magnet Synchronous Motors

Ruben Tapia-Olvera, Antonio Valderrabano-Gonzalez, *Senior Member, IEEE*, and Francisco Beltran-Carbajal

***Abstract*—Permanent Magnet Synchronous Motors (PMSM) are widely employed in high-performance industrial applications due to their high efficiency, high power density, and excellent controllability. The overall performance of PMSM drive systems is strongly influenced by the interaction between the control strategy and the power electronic converter. This paper presents a high-performance 84-pulse VSC integrated with an advanced speed control strategy for precise PMSM speed regulation. The proposed approach leverages the increased voltage resolution of the 84-pulse topology to improve dynamic response, reduce torque and voltage ripple, and enhance speed-tracking accuracy under variable operating conditions. A detailed simulation-based design of experiments (SBDoE) is conducted to evaluate the interaction between the control scheme and different converter topologies, including 36-pulse and 84-pulse configurations. The simulation model incorporates the electrical and mechanical dynamics of the PMSM, as well as the switching behavior of the converter, providing a realistic assessment of system performance under varying speed and load conditions. The results demonstrate that, compared with conventional lower-pulse converter topologies, the proposed configuration achieves smoother electromechanical behavior, reduced harmonic distortion, and improved tracking performance, making it well suited for high-precision PMSM drive applications.**

**Link to graphical and video abstracts, and to code:**
**https://latamt.ieeer9.org/index.php/transactions/article/view/10642**

***Index Terms*—Permanent magnet synchronous motor, Speed control, Power electronics, Multipulse converters.**

## I. Introduction

CURRENTLY, permanent magnet synchronous motors have an extensive range of applications. Their use is continuously growing, from industry to service and security tasks, mainly due to their operational versatility and the accurate trajectory tracking [1]. The availability of rare earths and the manufacture of motors in a wide range of power have been converted into the most desirable rotational machine.

These characteristics have favored their use in applications such as electric vehicles, robotics, and industrial automation, where strict performance criteria are required. However, speed regulation of these motors faces significant challenges associated with their nonlinear dynamics, parameter uncertainties, and the presence of disturbances in their operation, which can degrade the effectiveness of the control approaches that consider linear models and constant parameters [2], [3].

Additionally, most PMSM applications require a wide speed regulation range under time-varying disturbances, as well as compliance with physical current and voltage constraints, which places stricter demands on controller performance [4], [5]. In this context, current trends in PMSM speed control incorporate robust fixed-time strategies, advanced predictive control, and machine learning-based techniques, with the aim of improving dynamic performance and control robustness in the face of model uncertainties and real-time parameter variations [2], [3].

In the field of predictive motor control (PMC), two approaches can be distinguished: model-accurate and model-free. [6] and [7] propose improvements to predictive torque and flow control, aiming to reduce computational load and ripple using novel reference frames or vector modulation strategies. On the other hand, [2] and [8] have developed model-free schemes that employ extended state observers or local models, with the goal of reducing dependence on precise motor parameters. Furthermore, [1] integrates nonlinear thermal predictive control into the motor design phase using bayesian optimization techniques.

In this case, PMC-based approaches stand out for their ability to explicitly handle system operating constraints and for their performance during fast transients. However, their effectiveness is affected by their sensitivity to model mismatches. Although model-free approaches aim to mitigate this dependence, they lose the ability to accurately predict long-term physical conditions and depend critically on the observer's convergence speed, which can introduce phase delays at different operating speeds [2].

Regarding robust nonlinear control, sliding mode control (SMC) has evolved towards fixed-time convergence schemes to ensure performance independent of initial conditions. In [3] and [9], an adaptive fixed-time SMC combined with a disturbance observer is presented, ensuring error convergence under severe operating conditions. On the other hand, [10] introduces sliding surfaces inspired by supercritical bifurcation to mitigate chattering in the control signal caused by ideal controller switching, which can excite unmodeled dynamics, increase losses, and generate premature wear in actuators. Additionally, [11] addresses robustness from a hardware-oriented perspective, proposing an adaptive control scheme for low-

The associate editor coordinating the review of this manuscript and approving it for publication was Julio C. Rosas-Caro (*Corresponding author: Antonio Valderrabano-Gonzalez*).

R. Tapia-Olvera is with the Department of Electrical Energy, Universidad Nacional Autónoma de México, Mexico City, 04510, Mexico (e-mail: rtapia@fi-b.unam.mx).

Antonio Valderrabano-Gonzalez is with Universidad Panamericana, Facultad de Ingeniería, Álvaro del Portillo 49, Zapopan, Jalisco, 45010, México (e-mail: avalder@up.edu.mx).

F. Beltran-Carbajal is with the Department of Energy, Universidad Autónoma Metropolitana, Unidad Azcapotzalco, Mexico City, 02200, Mexico (e-mail: fbeltran@azc.uam.mx).

resolution Hall sensors in electric vehicles.

Finally, learning- and optimization-based approaches seek to incorporate real-time adaptation into the control scheme [12]. In [4], adaptive dynamic programming is employed, using a critical neural network and an actor neural network to approximate the cost function and the optimal controller, respectively. Meanwhile, in [13], radial basis function neural networks are used to approximate unknown dynamics under current constraints, while in [14] and [15], genetic algorithms and linear matrix inequalities are applied for the optimal tuning of fractional-order and passivity-based controllers, respectively.

However, each of these approaches has inherent advantages and limitations, leading to trade-offs between robustness, accuracy, adaptability, and computational complexity. Fixed-time SMC strategies [3], [15] offer a high level of theoretical robustness against disturbances and guarantee deterministic convergence times, characteristics particularly relevant in applications with safety requirements. However, the mathematical complexity of their control laws and the need for high-order observers increase the computational load and can hinder their implementation on embedded platforms. Additionally, mitigating high-frequency oscillations still depends on fine-tuning gains, which is often heuristic [16].

Self-learning based approaches offer greater adaptability to unmodeled dynamics and parametric variations, reducing reliance on explicit models and exact parameters. However, their practical application faces challenges related to ensuring stability during online learning, offline computational effort, and the additional computational load associated with continuous real-time parameter updates [3], [13].

Despite significant advances reported in the literature, critical limitations persist that hinder the widespread adoption of these advanced speed control strategies for PMSM. In particular, a gap exists between fixed-time SMC schemes and the actual physical constraints of the actuator, as most proposals assume non-saturated control actions, whereas in practical scenarios, inverter voltage and current saturation can degrade the performance and stability of these proposals. On the other hand, although self-learning based approaches offer superior adaptability, their computational load remains incompatible with high switching frequencies in conventional embedded hardware.

In this context, it is necessary to develop control schemes that integrate mathematical robustness, explicitly consider the physical constraints of the devices, and guarantee computational efficiency compatible with modern industrial hardware. It is very important to define the control strategy and the implementation in the electronic driver, which must cover complex behavior pattern of the load connected to the motor and uncertainties unmodeled in design stage.

Due to the limitations identified in existing approaches, this paper proposes an adaptive speed control strategy for PMSMs that integrates model-based design with data-driven adaptation. To clearly highlight the specific contributions of this work and its differentiation from related studies, the main features of the proposed methodology are summarized as follows:

The proposed adaptive speed control scheme:

- combines model-based control design with an online adaptive mechanism based on B-spline neural networks, enabling improved robustness while preserving a structured analytical formulation;
- enhances dynamic performance and tracking accuracy under varying speed and load torque conditions, as demonstrated through a systematic simulation-based evaluation;
- reduces dependence on precise motor parameters and unmodeled dynamics, allowing the controller to compensate for uncertainties without requiring their explicit inclusion during the initial design stage;
- maintains high performance even when the power electronic driver is not explicitly included in the control design, highlighting robustness against converter-induced effects;
- is validated in combination with multi-pulse converter topologies (36- and 84-pulse VSCs), demonstrating its applicability in high-performance PMSM drive systems with improved power quality.

## II. PMSM Representation for Speed Control Purposes

The direct-quadrature ($dq$) reference frame is preferred for the speed control design purposes of PMSM. Under this representation, it is possible to develop an adaptive 84-pulse speed control drive using B-spline neural networks as proposed in this research. The state space representation for the PMSM used is given by Equation (1):

$$\begin{aligned}
\frac{d}{dt}i_d &= -\frac{R_s}{L_d}i_d + \frac{n_pL_q}{L_d}i_q\omega + \frac{1}{L_d}u_d \\
\frac{d}{dt}i_q &= -\frac{R_s}{L_q}i_q - \frac{n_pL_d}{L_q}i_d\omega - \frac{n_p\lambda_m}{L_q}\omega + \frac{1}{L_q}u_q \\
\frac{d}{dt}\omega &= \frac{3}{2J}n_p\lambda_m i_q + \frac{3}{2J}n_p(L_d-L_q)i_di_q - \frac{b}{J}\omega - \frac{1}{J}\tau_L
\end{aligned} \tag{1}$$

The stator current and voltage in the direct or $d$ axis are represented as $i_d$ and $u_d$, respectively; the stator current and voltage in the quadrature or $q$ axis are represented as $i_q$ and $u_q$, respectively; the permanent magnet flux linkage is denoted by $\lambda_m$; $\omega$ is the mechanical angular speed and $\tau_L$ is the load torque. The motor parameters $L_d$ and $L_q$ stand for inductances on the $d$ and $q$ axes, respectively; $R_s$ denotes the stator resistance; $J$ and $b$ are the moment of inertia and the viscous friction coefficient, respectively; and $n_p$ is the number of pole pairs.

From a practical perspective, the design process begins considering the equilibrium points which represent possible steady state conditions of the PMSM. The equilibrium points in terms of the desired values for the output variables $\bar{y}_1 = \bar{\omega}$ and $\bar{y}_2 = \bar{i}_d$, as well as the equilibrium constant load torque $\bar{\tau}_L$, are calculated from Equation (1) as Equation 2:

$$\begin{aligned}
\bar{\omega} &= \bar{y}_1 \\
\bar{i}_d &= \bar{y}_2 \\
\bar{i}_q &= \frac{1}{\frac{3}{2J}n_p\lambda_m + \frac{3}{2J}n_p(L_d-L_q)\bar{y}_2(\frac{b}{J}\bar{y}_1 + \frac{1}{J}\bar{\tau}_L)}
\end{aligned} \tag{2}$$

## III. Design of Speed Control for PMSM

This section is focused on the differential flatness property of permanent magnet synchronous motors and using it to develop an efficient speed regulation strategy.

### A. Differential Flatness

The design for the control input $u$ is set up so that:

$$y_1 = \omega \to \omega^*, \quad y_2 = i_d \to 0$$

In this case, it is assumed that the state variables are available for feedback. Moreover, $\omega^*$ denotes the desired speed reference. For control design purposes, the dynamics of the electrical subsystem can be considered much faster than the dynamics of the mechanical subsystem. Sufficiently fast asymptotic convergence for $y_2 = i_d \to 0$ is guaranteed by the controller defined in Equation 3:

$$u_d = -\beta_d i_d - L_q n_p i_q \omega \tag{3}$$

where $\beta_d$ is a critical control parameter that must be optimally tuned to achieve smooth rotor speed regulation and ensure stability. Now, substituting $u_d$, Equation (3), into the equation for the dynamics of the current on the $d$-axis, (1),

$$\frac{d}{dt}i_d = -\frac{R_s}{L_d}i_d + \frac{n_p L_q}{L_d}i_q\omega + \frac{1}{L_d}(-\beta_d i_d - L_q n_p i_q \omega) \tag{4}$$

grouping common terms of Equation (4), results,

$$\frac{d}{dt}i_d = -\frac{1}{L_d}\left(R_s + \beta_d\right) i_d \tag{5}$$

Therefore, by selecting $\beta_d > -R_s$, asymptotic convergence is strictly guaranteed, $\lim_{t\to\infty} i_d = 0$. This can be demonstrated using the Lyapunov function

$$V_q(i_d) = \frac{1}{2}i_d^2 \tag{6}$$

where

$$\frac{d}{dt}V_q(i_d) = i_d\frac{d}{dt}i_d = -\frac{1}{L_d}(R_s+\beta_d)i_d^2 < 0, \quad i_d \neq 0 \tag{7}$$

For this scenario, we can hence consider that the dynamics of the controlled mechanical subsystem are given by

$$\begin{aligned} \frac{d}{dt}i_q &= -\frac{R_s}{L_q}i_q - \frac{n_p\lambda_m}{L_q}\omega + \frac{1}{L_q}u_q \\ \frac{d}{dt}\omega &= \frac{3}{2J}n_p\lambda_m i_q - \frac{b}{J}\omega - \frac{1}{J}\tau_L \\ y_1 &= \omega \end{aligned} \tag{8}$$

Model (8) represents a differentially flat system with flat output $y_1 = \omega$ [17]. The differential parameterization is given by

$$\begin{aligned} \omega &= y_1 \\ i_q &= \frac{2J}{3n_p\lambda_m}\frac{d}{dt}y_1 + \frac{2b}{3n_p\lambda_m}y_1 \\ u_q &= L_q\frac{d}{dt}i_q + R_s i_q + n_p\lambda_m\omega \end{aligned} \tag{9}$$

Considering the effect of load torque on the system trajectories, these equations, (9), are modified as follows,

$$\begin{aligned} \omega &= y_1 \\ i_q &= \frac{2J}{3n_p\lambda_m}\frac{d}{dt}y_1 + \frac{2b}{3n_p\lambda_m}y_1 + \frac{2}{3n_p\lambda_m}\tau_L \end{aligned} \tag{10}$$

substituting $i_q$, (10), in $u_d$ of Equation (9) results,

$$\begin{aligned} u_q &= \frac{2JL_q}{3n_p\lambda_m}\frac{d^2}{dt^2}y_1 + \left(\frac{2bL_q}{3n_p\lambda_m} + \frac{2JR_s}{3n_p\lambda_m}\right)\frac{d}{dt}y_1 \\ &+ \left(\frac{2bR_s}{3n_p\lambda_m} + n_p\lambda_m\right)y_1 + \frac{2L_q}{3n_p\lambda_m}\frac{d}{dt}\tau_L + \frac{2R_s}{3n_p\lambda_m}\tau_L \end{aligned} \tag{11}$$

Thus, the trajectories of the system variables in terms of the reference trajectories $y_1^* = \omega^*$ are given by,

$$\begin{aligned} \omega^* &= y_1^* \\ i_q^* &= \frac{2J}{3n_p\lambda_m}\frac{d}{dt}y_1^* + \frac{2b}{3n_p\lambda_m}y_1^* \\ u_q^* &= \frac{2JL_q}{3n_p\lambda_m}\frac{d^2}{dt^2}y_1^* + \left(\frac{2bL_q}{3n_p\lambda_m} + \frac{2JR_s}{3n_p\lambda_m}\right)\frac{d}{dt}y_1^* \\ &+ \left(\frac{2bR_s}{3n_p\lambda_m} + n_p\lambda_m\right)y_1^* + \frac{2L_q}{3n_p\lambda_m}\frac{d}{dt}\tau_L + \frac{2R_s}{3n_p\lambda_m}\tau_L \end{aligned}$$

Therefore, the perturbed dynamics of the flat output $y_1$ are governed by,

$$\begin{aligned} &\frac{d^2}{dt^2}y_1 + \left(\frac{R_s}{L_q} + \frac{b}{J}\right)\frac{d}{dt}y_1 + \left(\frac{bR_s}{JL_q} + \frac{3n_p^2\lambda_m^2}{2JL_q}\right)y_1 \\ &= \frac{3n_p\lambda_m}{2JL_q}u_q - \frac{1}{J}\frac{d}{dt}\tau_L - \frac{R_s}{JL_q}\tau_L \end{aligned} \tag{12}$$

The dynamics of the speed tracking error, $e_\omega = \omega - \omega^* = y_1 - y_1^*$, is obtained from Equation (12) as follows,

$$\begin{aligned} &\frac{d^2}{dt^2}e_\omega + \left(\frac{R_s}{L_q} + \frac{b}{J}\right)\frac{d}{dt}e_\omega + \left(\frac{bR_s}{JL_q} + \frac{3n_p^2\lambda_m^2}{2JL_q}\right)e_\omega \\ &= \frac{3n_p\lambda_m}{2JL_q}u_q - \frac{d^2}{dt^2}y_1^* - \left(\frac{R_s}{L_q} + \frac{b}{J}\right)\frac{d}{dt}y_1^* \\ &- \left(\frac{bR_s}{JL_q} + \frac{3n_p^2\lambda_m^2}{2JL_q}\right)y_1^* - \frac{1}{J}\frac{d}{dt}\tau_L - \frac{R_s}{JL_q}\tau_L \end{aligned} \tag{13}$$

In this paper, the following controller can be then derived for speed trajectory tracking $y_1^* = \omega^*$:

$$u_q = \frac{2JL_q}{3n_p\lambda_m}\left(\beta_{1,\omega}\frac{d}{dt}e_\omega + \beta_{0,\omega}e_\omega\right) - \varphi \tag{14}$$

with

$$\begin{aligned} \varphi = \frac{2JL_q}{3n_p\lambda_m}[&-\frac{d^2}{dt^2}y_1^* - \left(\frac{R_s}{L_q} + \frac{b}{J}\right)\frac{d}{dt}y_1^* \\ &- \left(\frac{bR_s}{JL_q} + \frac{3n_p^2\lambda_m^2}{2JL_q}\right)y_1^* - \frac{1}{J}\frac{d}{dt}\tau_L - \frac{R_s}{JL_q}\tau_L] \end{aligned} \tag{15}$$

where $\beta_{1,\omega}$ and $\beta_{0,\omega}$ represent the control gains. This is a critical stage in the proposed controller design, as the optimal selection of these control gains is essential to guarantee the asymptotic convergence of the motor speed control strategy.

The closed-loop dynamics of the velocity tracking error is given by,

$$\frac{d^2}{dt^2}e_\omega + (\alpha_{1,\omega} + \beta_{1,\omega})\frac{d}{dt}e_\omega + (\alpha_{0,\omega} + \beta_{0,\omega})e_\omega = 0 \quad (16)$$

where

$$\alpha_{1,\omega} = \frac{R_s}{L_q} + \frac{b}{J}, \quad \alpha_{0,\omega} = \frac{bR_s}{JL_q} + \frac{3n_p^2\lambda_m^2}{2JL_q} \quad (17)$$

Defining the following state variables: $e_{1,\omega} = e_\omega$ and $e_{2,\omega} = \dot{e}_\omega$, the tracking error dynamics is formulated in state-space as

$$\begin{aligned} \frac{d}{dt}e_{1,\omega} &= e_{2,\omega} \\ \frac{d}{dt}e_{2,\omega} &= -(\alpha_{0,\omega} + \beta_{0,\omega})e_{1,\omega} - (\alpha_{1,\omega} + \beta_{1,\omega})e_{2,\omega} \end{aligned} \quad (18)$$

Hence, selecting $\beta_{0,\omega} > -\alpha_{0,\omega},\ \beta_{1,\omega} > -\alpha_{1,\omega}$, asymptotic tracking of the speed reference $\omega^*$ is guaranteed:

$$\lim_{t\to\infty} e_{1,\omega} = 0 \Rightarrow \lim_{t\to\infty} y_1 = y_1^* = \omega^* \quad (19)$$

Note that $\alpha_{0,\omega}$ and $\alpha_{1,\omega}$ depend on the correct values of the motor parameters and consequently $\beta_{0,\omega}$ and $\beta_{1,\omega}$. However, an important aspect to consider is ensuring that these values are available. In this context, to mitigate the uncertainties inherent in these parameters, an adaptive tuning strategy is implemented, as detailed in subsection III-B.

Now, the asymptotic tracking of the speed reference can be demonstrated from the LaSalle's Theorem by considering the Lyapunov function

$$V_\omega(e_{1,\omega}, e_{2,\omega}) = \frac{1}{2}(\alpha_{0,\omega} + \beta_{0,\omega})e_{1,\omega}^2 + \frac{1}{2}e_{2,\omega}^2 \quad (20)$$

where

$$\frac{d}{dt}V_\omega(e_{1,\omega}, e_{2,\omega}) = -(\alpha_{1,\omega} + \beta_{1,\omega})e_{2,\omega}^2 \leq 0 \quad (21)$$

In summary, the controllers are given by,

$$\begin{aligned} u_d &= -\beta_d i_d - L_q n_p i_q \omega \\ u_q &= -\frac{2JL_q}{3n_p\lambda_m}\left(\beta_{1,\omega}\frac{d}{dt}e_\omega + \beta_{0,\omega}e_\omega\right) - \varphi \end{aligned} \quad (22)$$

with

$$\varphi = \frac{2JL_q}{3n_p\lambda_m}\left(-\frac{d^2}{dt^2}y_1^* - \alpha_{1,\omega}\frac{d}{dt}y_1^* - \alpha_{0,\omega}y_1^* - \frac{1}{J}\frac{d}{dt}\tau_L \right. \\ \left. -\frac{R_s}{JL_q}\tau_L\right)$$

The control parameters can be selected using the following Hurwitz polynomials with $p_d, p_\omega > 0$:

$$\begin{aligned} P_d(s) &= s + p_d \\ P_\omega(s) &= (s + p_\omega)^2 = s^2 + 2p_\omega s + p_\omega^2 \end{aligned} \quad (23)$$

To compute these control parameters, the positive numerical values of $R_s$, $\alpha_{0,\omega}$ and $\alpha_{1,\omega}$ might be omitted resulting: $\beta_d = p_d$, $\beta_{0,\omega} = p_w^2$ and $\beta_{1,\omega} = 2p_\omega$. For this study, a constant value of 20 to $\beta_d$ has been defined, and the dynamic update task is extended in the subsection III-B for $\beta_{1,\omega}$, $\beta_{0,\omega}$, $\alpha_{1,\omega}$ and $\alpha_{0,\omega}$. In this work, it was decided to leave $\beta_d$ constant to highlight that some gains can be left constant with approximate values and only some control gains can be dynamically updated guaranteeing an adequate overall performance of the VSC.

However, controllers (22) based on Lyapunov theory are highly dependent on motor parameters; any changes to them may degrade the controller's behavior even with the possibility of having a faulty performance. Thus, an efficient strategy is necessary to include after the speed controller design stage presented in this section. Moreover, at this moment no details or model of the power electronics driver have been included, which is extremely relevant to ensure the correct operation of the PMSM in high demand and precision scenarios. In the following sections, the incorporation of B-spline neural networks and the 84-Pulse VSC for the proposed robust adaptive PMSM control drive technology is discussed.

### B. Improved Controller avoiding Parameter Dependency

In this article, it is presented an improved controller based on B-spline neural networks. There are three main aspects which can cover with a correct design of this new adaptive controller approach: 1) to evade the high dependency on motor parameters which change over time; 2) due that in the control design stage no details of the power electronics driver have been included it is necessary to reject the inherent uncertainties to this irreplaceable component; 3) to cope with various uncertainties and nonlinear variations in load torque or highly demanded scenarios associated with the motor applications.

Fig. 1 illustrates the general architecture of the proposed PMSM drive system. The permanent magnet synchronous motor (PMSM) is supplied by a multipulse VSC, which provides the required three-phase voltages for motor operation. The gate signals of the converter are generated by a control block that processes the measured electrical and mechanical variables of the system. The three-phase stator currents are measured and transformed into the synchronous dq reference frame, enabling the implementation of the control strategy in a decoupled form. In addition, a speed sensor is used to monitor the rotor angular velocity, which is continuously compared with the reference speed signal. The speed tracking error is used as an input to an adaptive mechanism based on gain adjustment, which dynamically updates the controller parameters. These adaptive gains are then fed into the control block, allowing the generation of appropriate control actions to ensure accurate speed tracking and robust performance under varying operating conditions. This integrated structure highlights the interaction between the multipulse power converter, the PMSM, and the adaptive control scheme, forming a closed-loop system capable of high-performance operation.

As can be seen in section III-A the performance of designed controller depends on four constants $\beta_{0,\omega}$, $\beta_{1,\omega}$, $\alpha_{0,\omega}$, $\alpha_{1,\omega}$. Therefore, it is necessary to have available the specific values of motor parameters which itself is a very hard issue. Furthermore, any parameter variation can degrade controller performance and potentially lead to system malfunction. Finally, if the system model contains unmodeled dynamics or omissions, the accuracy results are not guaranteed. Thus, in this paper, these four gains were initially determined by approximate

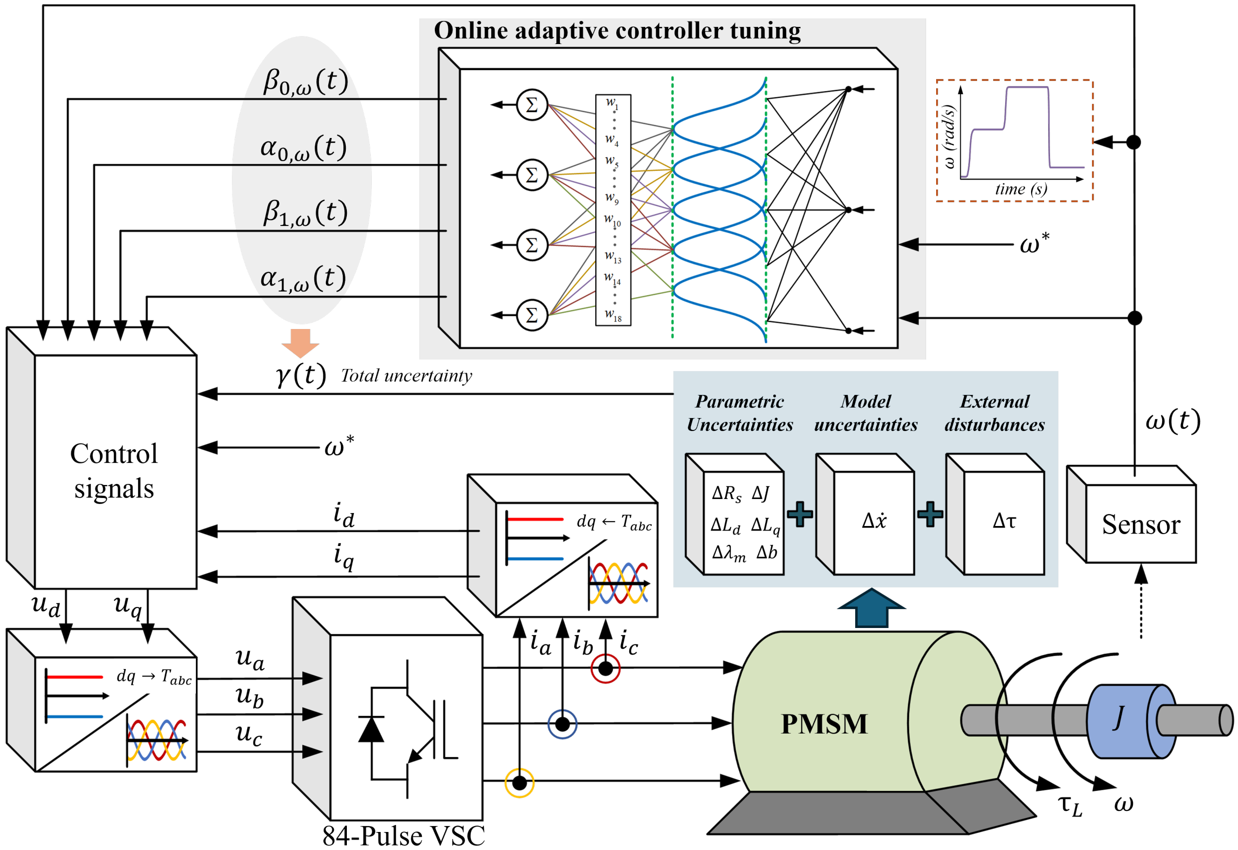


Fig. 1. General system scheme of the proposed PMSM drive with multipulse converter and adaptive control.

parameters; it now becomes dynamic variables adaptive by a B-spline neural structure Fig. 2.

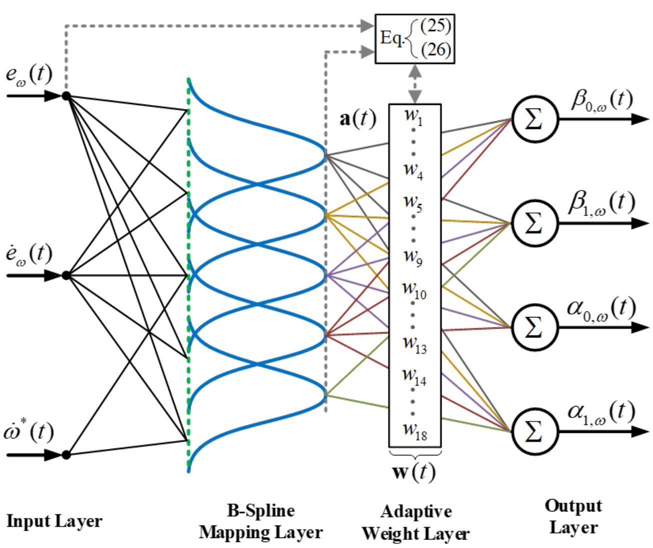


Fig. 2. Scheme for adjusting adaptive gains.

The architecture consists of three input variables: the speed error, $e_\omega$, its time derivative, $\dot{e}_\omega$, and the derivative of the reference speed trajectory, $\dot{\omega}^*$. These inputs are selected considering the control law developed in section III-A. The output variables are the corresponding required gains, and the activation functions are B-spline class to ensure smooth functional approximation. Denoting the output of the basis functions as $\mathbf{a}^t$, the controller gains are updated as follows,

$$gains = \mathbf{a}^t\mathbf{w} \tag{24}$$

In this case, were necessary 18 synaptic weighs to guarantee control law convergence. This structure was optimized through offline training under steady state operating conditions, using the nominal motor parameters as a baseline for the initial configuration.

The initial value of the weighing vector, $\mathbf{w}^0$, was determined, knowing the gain values for the steady-state condition of the motor and the respective values of the inputs: the speed error, its time derivative and, the derivative of the reference speed trajectory. These last values are the inputs for the B-spline basis functions, (24). With this procedure performed offline, now it is necessary to define the scheme for updating the synaptic weights (25). This real-time update law ensures that the controller can compensate for dynamic uncertainties and parameter variations during operation.

$$\begin{bmatrix} \mathrm{w}_1 \\ \mathrm{w}_2 \\ \vdots \\ \mathrm{w}_{18} \end{bmatrix}^{k+1} = \begin{bmatrix} \mathrm{w}_1 \\ \mathrm{w}_2 \\ \vdots \\ \mathrm{w}_{18} \end{bmatrix}^{k} + \begin{bmatrix} \Delta\mathrm{w}_1 \\ \Delta\mathrm{w}_2 \\ \vdots \\ \Delta\mathrm{w}_{18} \end{bmatrix}^{k} \tag{25}$$

In online operation, any change on the three inputs, Fig. 2, it is reflected in the output of the basis functions. Consequently, the weight vector must be updated online to maintain accurate control and adapt to these changes. To achieve this, an instantaneous learning rule is used as presented in (26):

$$\Delta \mathbf{w}^k = \frac{\eta e_\omega^k(t)}{\|\mathbf{a}^k(t)\|_2^2}\mathbf{a}^k(t) \tag{26}$$

where $k$ is the actual value; $e_\omega$ is the current speed error; $\mathbf{a}(t)$ is the output of the basis functions and; $\eta$ is the learning rate determined as a previous step in the offline training.

These gains, $\beta_{0,\omega}$, $\beta_{1,\omega}$, $\alpha_{0,\omega}$, $\alpha_{1,\omega}$, update characteristics result in a robust control scheme suitable for PMSM speed regulation. The controller effectively compensates for parametric variations, unmodeled phenomena, load torque disturbances, and operation across a wide speed range. In this specific case, not including the VSC was intentional, as incorporating a detailed converter model, particularly for high-pulse configurations, introduces significant computational complexity and increases the burden associated with controller tuning and implementation.

To address the resulting uncertainties, the proposed adaptive strategy based on B-spline neural networks is employed to compensate for unmodeled dynamics introduced by the power electronic stage. To validate this approach, two converter configurations with different pulse numbers (36-pulse and 84-pulse VSCs) have been analyzed. These configurations represent operating conditions with different harmonic distortion levels, allowing the evaluation of the controller under both relatively high-distortion and high-quality voltage scenarios.

The results presented in Section IV demonstrate that the adaptive scheme maintains high speed tracking performance in both cases, confirming its ability to mitigate converter-induced nonlinearities and uncertainties without requiring an explicit converter model during the design phase. Additionally, the manuscript clarifies that the control strategy is initially derived from a model-based formulation (Section III-A), while robustness and performance are ensured through the dynamic retuning of control gains enabled by the adaptive mechanism (Section III-B).

## IV. Simulation-Based Evaluation of the PMSM Drive Performance

To evaluate the performance of the controller and VSCaltogether, a simulation-based design of experiments (SBDoE) was conducted. The simulation model of the three-phase PMSM drive was implemented with the detailed electrical and mechanical dynamics of the machine in Matlab/Simulink 25.1 environment, as well as the switching behavior of the converter implemented in PLECS 4.9.8. A series of operating scenarios was simulated by varying the rotational speed and the applied load torque through multiple profile configurations, thereby enabling a comprehensive assessment of the controller's behavior under diverse and dynamically demanding conditions.

The analyzed simulation cases are summarized as follows:

- 1. Baseline response — without the VSC and without the neural network. This condition is defined as the reference case for evaluating the integration of the Electromechanical Drive System (EMDS). In this scenario, the frequency and voltage modules are represented by ideal sinusoidal signals, providing the exact input conditions required by the control stage to achieve the desired speed and torque trajectories.
- 2. Response with a 36-pulse VSC, without the neural network. In contrast, this scenario uses a VSC of a good quality that can generate a $5.1479\%$ [18] of harmonic distortion at the output. The pulse jumps can provoke slight differences from the baseline case.
- 3. Response with an 84-pulse VSC, without the neural network. On the other hand, using an 84-pulses VSC can bring a very low harmonic distortion, around $2.5\%$ [19]. This is a high quality generated signal, but the pulse jumps, even though are of a shorter amplitude, are more frequent, so it is needed to verify its influence on the general system.
- 4. Response with a 36-pulse VSC, including the neural network. This scenario includes the use of the 36-pulse VSC along with the BSpline neural network tuned to reduce variations on the speed profile.
- 5. Response with an 84-pulse VSC, including the neural network. For this case, the response is computed by using the high quality VSC of 84-pulses but also the BSpline tuned for the previous conditions, so, no new tunning was developed for having other response.

The VSCs considered in the SBDoE are derived from the conventional twelve-pulse converter structure. The 36-pulse and 84-pulse configurations are obtained by combining the basic twelve-pulse topology with multi-level input stages and appropriate reinjection transformers. Specifically, the 84-pulse VSC is implemented using a seven-level single-phase inverter stage that feeds the twelve-pulse converter, enabling a sort of pulse product and producing a higher number of voltage steps, and consequently, the improved harmonic cancellation. In contrast, the 36-pulse configuration employs a three-level single-phase inverter as the input stage, which is easier to build and results in a lower number of effective pulses and comparatively higher harmonic distortion, but in any case, the result is a closer version to the sinusoidal signal. In both cases, the transformer turns ratios and phase shifts are selected to minimize THD at the converter output. A detailed description of the 84-pulse converter topology, including the seven-level structure, switching patterns, and harmonic performance, can be found in [20]. Similarly, the implementation and harmonic optimization of the 36-pulse configuration are described in [18].

The resulting speed, torque, voltage, and active power profiles are presented in the figures of this section. These plots illustrate the system's ability to track speed references, maintain torque stability, and manage the converter output voltage to achieve effective energy conversion. The results demonstrate consistent coordination between the controller and the converter, confirming the robustness and efficiency of the proposed drive strategy across the tested operating range.

On this voltage-based controller, the voltage waveform produced by a VSC is inherently discontinuous, composed of stiff, stair-cased voltage transitions that approximate a sinusoidal reference. These changes in voltage introduce harmonic distortion into the motor. As a result, the motor windings experience non-sinusoidal currents that generate torque ripple, additional losses, and increase the acoustic noise. When the total harmonic distortion (THD) of the converter output is high, these effects are amplified—leading to stronger electromagnetic stresses, higher temperature rise, and potential degradation of insulation or bearing systems. Therefore, minimizing the harmonic content of the converter output is essential to ensure smooth torque production and long-term reliability of the motor drive.

A comparison of the speed obtained with the five cases of the SBDoE is provided in Fig. 3. In contrast to the baseline reference case, the inclusion of the VSC introduces a noticeable speed offset when the torque is changed. This offset is increased as the commanded speed becomes higher. When the B-spline neural network is incorporated into the control structure, this offset is effectively mitigated, yielding a response that closely follows the speed reference. The reduction in offset is particularly significant when using the 84-pulse VSC, which exhibits the smallest deviation among the evaluated configurations.

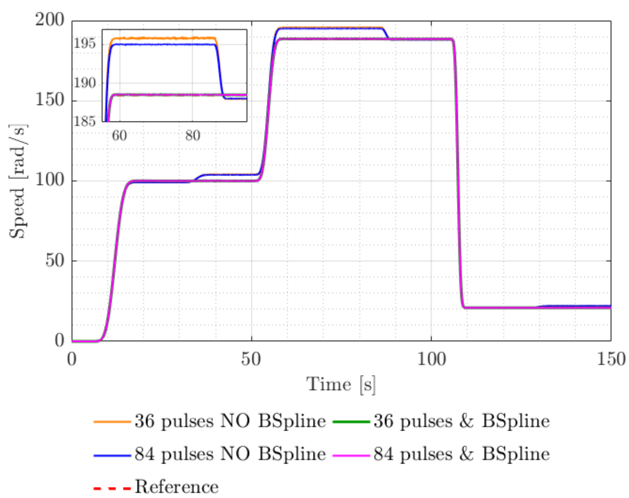


Fig. 3. Speed profile comparison for the SBDoE performed, and close-up of the main speed variations.

On the other hand, Fig. 4, presents the torque variations expected on the dotted line as reference. By adding the VSC to generate the required voltage, some elongations take place when a variation on the speed is required, obtaining better response when the combination of the 84 pulses VSC and the BSpline are used.

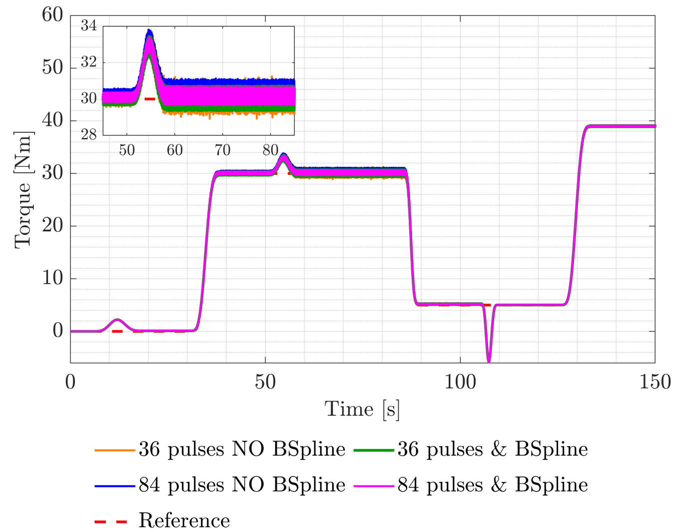


Fig. 4. Torque profile comparison for the SBDoE performed, and close-up of the main torque variations.

In order to follow the voltage amplitude, the EMDS uses the voltage module defined by (27). Here $V_m$ represents the module of the voltage, and $v_a$, $v_b$ and $v_c$ are the phase voltages required to track the instantaneous speed of the PMSM. By processing this signal, the EMDS accounts not only for the dynamic speed reference but also for variations in load torque and converter operating conditions, ensuring accurate closed-loop control. The required voltage module is depicted in Fig. 5. Again the reference voltage is plotted in dotted line while the best approximation is obtained with the 84 pulses VSC and the BSpline working together but the required value is higher than the reference with some oscillations.

$$V_m = \sqrt{{v_a}^2 + {v_b}^2 + {v_c}^2} \tag{27}$$

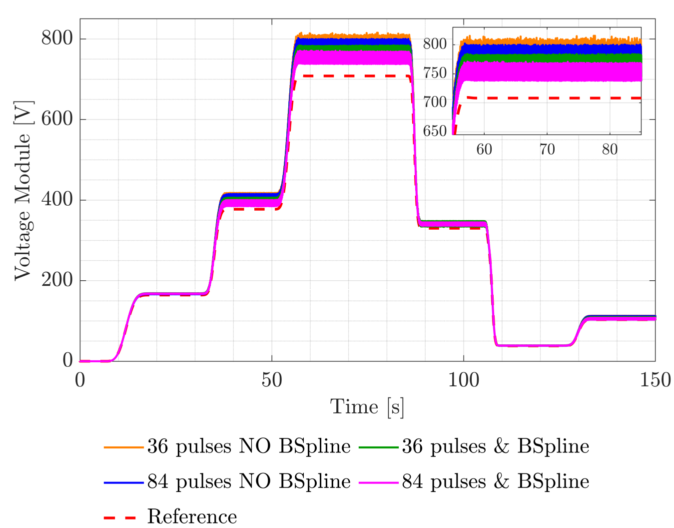


Fig. 5. Voltage profile comparison for the SBDoE performed and close-up of the main voltage variations.

The profile for the active power presents a slightly weird behavior as the ripple is lower when no neural network is used, but also the 84 pulses VSC has better conditions than the 36 pulses VSC. This can be observed in Fig. 6.

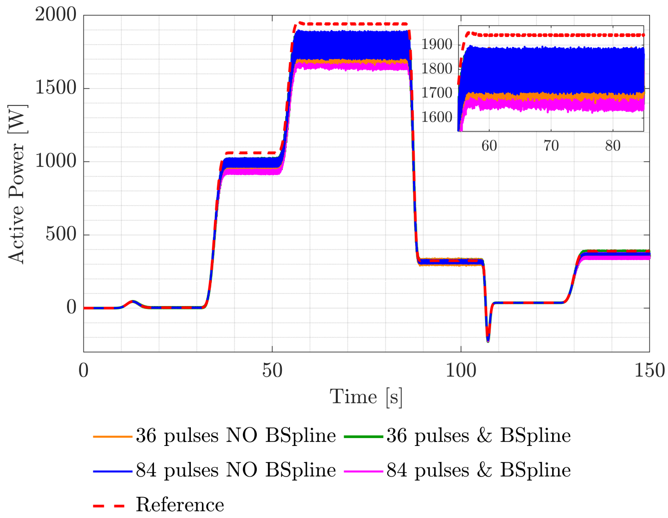


Fig. 6. Active Power profile comparison for the SBDoE performed and close-up of the main active power variations.

By combining the variations in speed and torque, the operating profile can be divided into seven steady-state sections. The first section corresponds to the motor at standstill, where no mechanical energy is demanded. The performance characteristics and merit figures obtained for Sections 2 through 7 are summarized in Table I. Based on these results, the configuration that achieves the best speed-tracking performance is the system using the 36-pulse VSC in combination with the B-spline neural network. This arrangement outperforms the 84-pulse VSC with neural enhancement by a small margin, although it does so at the expense of higher torque, voltage, and power ripple.

This performance was achieved by dynamically adapting the controller gains, $\beta_{0,\omega}$, $\beta_{1,\omega}$, $\alpha_{0,\omega}$, and $\alpha_{1,\omega}$ as can be seen in Fig. 7. These adaptations are driven by real speed and load requirements, ensuring robust motor response in a wide range of operating conditions without redesigning the control strategy. The synaptic weights convergence is presented in Fig. 8. The convergence of all synaptic weights ensures that the speed error, $e_\omega$, asymptotically approaches zero. Consequently, the proposed controller effectively compensates system uncertainties, including electronic driver dynamics and drastic variations in both reference and load torque. The proposed strategy exhibits selective adaptation; rather than a global update, only a subset of synaptic weights is adjusted in accordance with the learning rule. This adaptation is used to compensate possible uncertainties and and non-linearities in the motor-inverter system while maintaining the stability of previously learned states, Figs. 7 and 8.

The proposed control strategy followed in this work has been developed with practical implementation in mind, even though the presented results are based on simulation. The low computational complexity of the adaptive mechanism based on B-spline neural networks makes it suitable for real-time applications. The update of synaptic weights uses an instantaneous learning rule, as described in Eqs. (24)–(26), enabling efficient online adaptation without requiring intensive numerical optimization.

The computational burden associated with the adaptive update results in an execution time of approximately 0.091 ms per iteration, evaluated in a real-time processing environment. This processing time supports the feasibility of real-time implementation, according to typical sampling periods used in high-performance motor drive systems. The control strategy was intentionally designed without requiring a detailed model of the VSC, reducing the modeling complexity and simplifying the controller tuning, particularly in high-pulse converter configurations where the number of switching devices significantly increases the computational burden. The adaptive scheme compensates for converter-induced nonlinearities and uncertainties during operation, as demonstrated by the results obtained with both 36-pulse and 84-pulse configurations.

In addition, the proposed methodology does not require precise knowledge of motor parameters. The use of approximate values during the initial design and offline training stages simplifies the methodology, while the adaptive mechanism dynamically adjusts the control gains to compensate for parameter variations and unmodeled dynamics in real time. These features reduce the effort and enhance the robustness and scalability of the proposed approach for practical PMSM drive applications.

## V. Conclusions

This proposal has employed a simulation-based design of experiments (SBDoE) to identify the most suitable option for speed regulation of a three-phase PMSM under simultaneous variations in torque and speed. Since the primary controlled variable is the mechanical speed, the trade-off analysis shows that the 36-pulse VSC with B-spline assistance achieves the highest tracking accuracy. However, the 84-pulse configuration provides a favorable trade-off between speed tracking accuracy and output waveform quality. This characteristic makes it particularly suitable for high-performance applications where precise PMSM speed regulation and reduced ripple are critical. The results obtained from both converter configurations validate the effectiveness of the proposed adaptive controller in handling high-order switching dynamics without requiring an explicit and detailed model of the power electronic stage. This demonstrates the capability of the control strategy to maintain robust performance under varying converter conditions, supporting its applicability to different drive system configurations. The results presented in this work have been validated through detailed simulation studies that incorporate both the electromechanical dynamics of the PMSM and the switching behavior of the power electronic converter. These simulations were designed to reflect realistic operating conditions, including variations in speed and load torque, as well as the interaction with multi-pulse converter topologies. Although full experimental validation is beyond the scope of this study, a preliminary laboratory-level implementation of the adaptive controller has been carried out, confirming its feasibility for real-time deployment. Furthermore, the proposed adaptive control strategy is not restricted to a specific VSC configuration and demonstrates the ability to accommodate variations in converter topology and operating conditions, highlighting its potential applicability in practical PMSM drive systems.

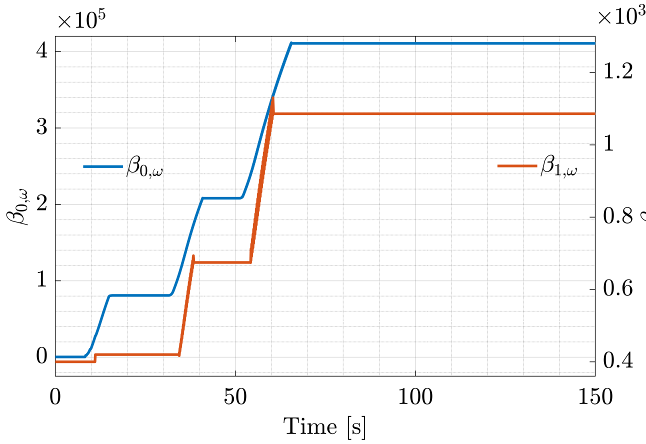


(a) Time evolution of adaptive gains $\beta_{0,\omega}$ and $\beta_{1,\omega}$.

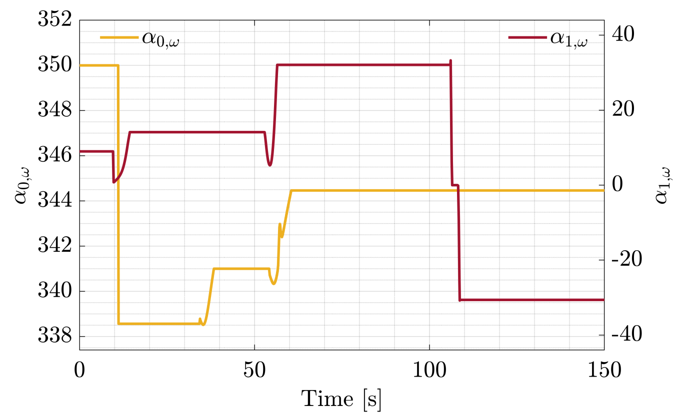


(b) Time evolution of adaptive gains $\alpha_{0,\omega}$ and $\alpha_{1,\omega}$.

Fig. 7. Adaptive gains evolution

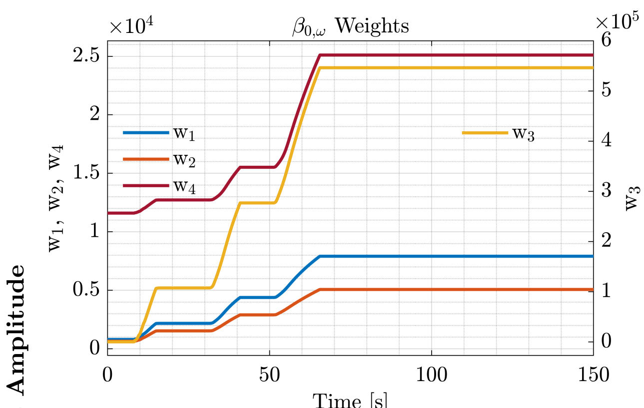


(a) Time evolution of $\beta_{0,\omega}$ synaptic weights

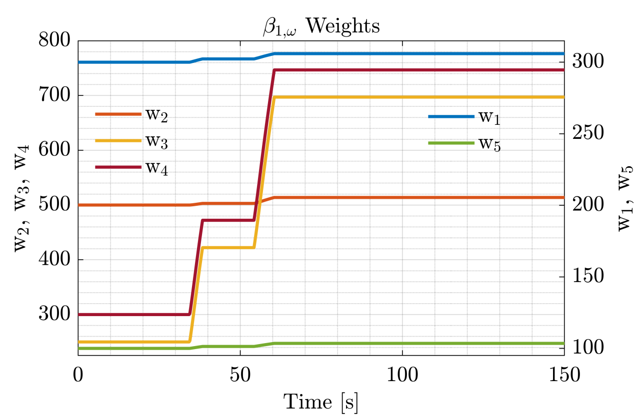


(b) Time evolution of $\beta_{1,\omega}$ synaptic weights

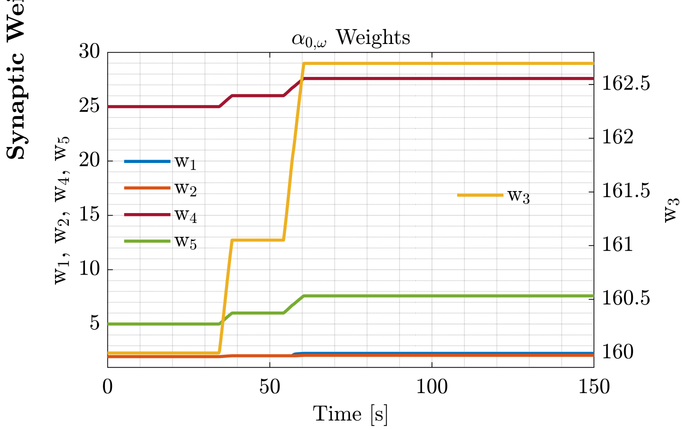


(c) Time evolution of $\alpha_{0,\omega}$ synaptic weights

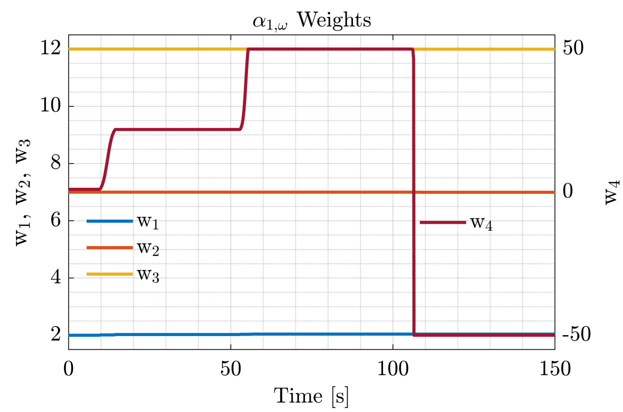


(d) Time evolution of $\alpha_{1,\omega}$ synaptic weights

Fig. 8. Adaptive weights convergence

TABLE I
COMPARISON OF MERIT FIGURES OBTAINED FROM THE SBDOE FOR THE SPEED CONTROL PROPOSED

| Feature and Performance | Reference | 36 pulses VSC NO BSpline | 84 pulses VSC NO BSpline | 36 pulses VSC & BSpline | 84 pulses VSC & BSpline |
|---|---|---|---|---|---|
| | | | **Section 2** | | |
| **Steady state speed** | 100.000 | 99.130 | 99.221 | 100.035 | 100.035 |
| **Deviation from reference** | 0 | −0.870 | −0.779 | 0.035 | 0.035 |
| **Maximum torque ripple** | 0 | 0.056 | 0.068 | 0.024 | 0.025 |
| **Average voltage** | 164.380 | 166.678 | 166.403 | 168.202 | 167.744 |
| **Maximum voltage ripple** | 0.001 | 0.628 | 0.388 | 1.386 | 1.146 |
| **Average power** | 3.286 | 2.563 | 2.668 | 2.648 | 2.747 |
| **Maximum power ripple** | 0.012 | 4.838 | 3.935 | 4.705 | 2.806 |
| | | | **Section 3** | | |
| **Steady state speed** | 100.000 | 104.126 | 103.801 | 100.034 | 100.034 |
| **Deviation from reference** | 0 | 4.126 | 3.801 | 0.034 | 0.034 |
| **Maximum torque ripple** | 0 | 0.952 | 0.894 | 0.674 | 0.533 |
| **Average voltage** | 377.407 | 410.517 | 407.273 | 393.783 | 392.848 |
| **Maximum voltage ripple** | 0 | 13.951 | 13.925 | 20.335 | 15.598 |
| **Average power** | 1060.399 | 991.305 | 998.511 | 967.305 | 961.542 |
| **Maximum power ripple** | 1.852 | 64.397 | 58.991 | 109.748 | 96.099 |
| | | | **Section 4** | | |
| **Steady state speed** | 188.496 | 195.803 | 195.012 | 188.536 | 188.537 |
| **Deviation from reference** | 0 | 7.307 | 6.516 | 0.040 | 0.041 |
| **Maximum torque ripple** | 0 | 2.303 | 1.755 | 1.366 | 1.027 |
| **Average voltage** | 708.192 | 788.927 | 779.171 | 756.491 | 754.844 |
| **Maximum voltage ripple** | 0.002 | 49.225 | 36.351 | 45.675 | 33.199 |
| **Average power** | 1941.462 | 1789.307 | 1810.054 | 1753.645 | 1734.712 |
| **Maximum power ripple** | 3.247 | 223.556 | 200.109 | 242.225 | 213.444 |
| | | | **Section 5** | | |
| **Steady state speed** | 188.496 | 187.979 | 188.042 | 188.518 | 188.518 |
| **Deviation from reference** | 0 | −0.517 | −0.454 | 0.022 | 0.022 |
| **Maximum torque ripple** | 0 | 0.471 | 0.250 | 0.206 | 0.121 |
| **Average voltage** | 330.137 | 340.144 | 339.034 | 341.065 | 339.846 |
| **Maximum voltage ripple** | 0 | 9.098 | 5.234 | 14.717 | 8.620 |
| **Average power** | 323.368 | 316.571 | 317.836 | 317.630 | 318.930 |
| **Maximum power ripple** | 0.310 | 51.444 | 29.779 | 38.809 | 23.368 |
| | | | **Section 6** | | |
| **Steady state speed** | 20.944 | 20.975 | 20.976 | 20.946 | 20.946 |
| **Deviation from reference** | 0 | 0.031 | 0.032 | 0.002 | 0.002 |
| **Maximum torque ripple** | 0 | 0.056 | 0.026 | 0.021 | 0.015 |
| **Average voltage** | 38.229 | 38.967 | 38.890 | 38.918 | 38.839 |
| **Maximum voltage ripple** | 0.013 | 0.757 | 0.458 | 1.350 | 0.762 |
| **Average power** | 36.536 | 36.380 | 36.421 | 36.340 | 36.389 |
| **Maximum power ripple** | 0.036 | 1.144 | 0.647 | 0.953 | 0.545 |
| | | | **Section 7** | | |
| **Steady state speed** | 20.944 | 22.105 | 22.087 | 20.948 | 20.948 |
| **Deviation from reference** | 0 | 1.161 | 1.143 | 0.004 | 0.004 |
| **Maximum torque ripple** | 0 | 0.249 | 0.238 | 0.238 | 0.160 |
| **Average voltage** | 103.429 | 111.338 | 110.985 | 105.862 | 105.675 |
| **Maximum voltage ripple** | 0 | 2.745 | 2.715 | 6.567 | 4.604 |
| **Average power** | 388.992 | 368.740 | 369.419 | 361.359 | 356.394 |
| **Maximum power ripple** | 0.717 | 9.379 | 9.241 | 54.195 | 42.357 |

## DECLARATIONS

### *Conflict of Interest*

The authors declare that they have no conflict of interest.

## ACKNOWLEDGMENTS

This work was supported by the Programa de Apoyo a Proyectos de Investigación e Innovación Tecnológica (PAPIIT) under Grant UNAM-DGAPA-PAPIIT-IN115123.

## REFERENCES

[1] C. Wellmann, A. R. Khaleel, T. Brinkmann, A. Wahl, C. Monissen, M. Eisenbarth, and J. Andert, "Electric machine co-optimization for ev drive technology development: Integrating bayesian optimization and nonlinear model predictive control," *eTransportation*, vol. 23, p. 100392, 2025, DOI: 10.1016/j.etran.2024.100392.

[2] Y. Liu, G. Zhou, L. Guo, and Z. Sun, "Eso-based direct model-free adaptive predictive compensation control for permanent magnet synchronous motors," *IEEE Access*, vol. 13, pp. 7837–7849, 2025, DOI: 10.1109/ACCESS.2025.3526282.

[3] R. Xu, J. Liu, X. Lin, S. Cai, Z. Liu, Y. Gao, and L. Wu, "Adaptive fixed-time control for permanent magnet synchronous motors with unknown

disturbances," *IEEE Transactions on Power Electronics*, vol. 41, no. 1, pp. 291–302, 2026, DOI: 10.1109/TPEL.2025.3595734.

[4] Z.-X. Fan, S. Li, and J. Su, "Adaptive dynamic programming for pmsm control under safety, robustness, and optimality constraints," *IEEE Transactions on Systems, Man, and Cybernetics: Systems*, vol. 55, no. 4, pp. 2724–2733, 2025, DOI: 10.1109/TSMC.2024.3510544.

[5] Z. Cao, J. Mao, X. Dong, R. Madonski, C. Zhang, and J. Yang, "Composite generalized dynamic predictive control with self-tuning horizon for wide-range speed regulation of pmsm drives," *IEEE Transactions on Energy Conversion*, vol. 39, no. 1, pp. 659–674, 2024, DOI: 10.1109/TEC.2023.3329931.

[6] J. He, Z. Li, G. Wu, and R. Tang, "Model predictive stator flux control of permanent magnet synchronous motor based on vector duty ratio modulation," *IEEE Access*, vol. 13, pp. 11 295–11 306, 2025, DOI: 10.1109/ACCESS.2024.3433508.

[7] X. Qu, Q. Wang, C. Peng, and Z. Li, "Novel deadbeat direct torque and flux control for interior permanent magnet synchronous motor," *Electrical Engineering*, vol. 107, no. 2, pp. 1607–1616, Feb 2025, DOI: 10.1007/s00202-024-02606-2.

[8] X. Liu, H. Yang, S. Cai, H. Lin, F. Yu, and Y. Yang, "Improved predictive current controller for variable flux memory machine drives considering magnetization state manipulating operations," *IEEE Journal of Emerging and Selected Topics in Power Electronics*, vol. 13, no. 2, pp. 1406–1417, 2025, DOI: 10.1109/JESTPE.2025.3529984.

[9] H. M. Trinh, T. H. Nguyen, T. T. Nguyen, and J. W. Jeon, "Robust adaptive learning rate neural network state observer based fixed-time sliding mode control of a permanent magnet synchronous motor," *IEEE Transactions on Power Electronics*, vol. 41, no. 2, pp. 1826–1840, 2026, DOI: 10.1109/TPEL.2025.3602407.

[10] J. Kim, S. Choi, and D. Yun, "Supercritical sliding mode control for position tracking of pmsm with disturbance rejection," *IEEE Transactions on Power Electronics*, vol. 41, no. 1, pp. 13–24, 2026, DOI: 10.1109/TPEL.2025.3603876.

[11] S. Singh, A. Arya, S. Anand, and K. Chatterjee, "Rotor position error based adaptive controller for improved average torque in pmsm drives for electric vehicles," *IEEE Transactions on Transportation Electrification*, pp. 1–1, 2025, DOI: 10.1109/TTE.2025.3638052.

[12] A. G. de Castro, P. R. U. Guazzelli, C. M. R. de Oliveira, W. C. d. A. Pereira, G. T. de Paula, and J. R. B. d. A. Monteiro, "Optimized current waveform for torque ripple mitigation and mtpa operation of pmsm with back emf harmonics based on genetic algorithm and artificial neural network," *IEEE Latin America Transactions*, vol. 18, no. 09, pp. 1646–1655, 2020, DOI: 10.1109/TLA.2020.9381808.

[13] J. Zhang, W. Ren, J. Li, and X.-M. Sun, "Adaptive neural asymptotic tracking control for pmsm systems under current constraints and unknown dynamics," *IEEE Transactions on Circuits and Systems II: Express Briefs*, vol. 71, no. 2, pp. 777–781, 2024, DOI: 10.1109/TCSII.2023.3311802.

[14] H. Fan, H. Wei, D. Xu, and Y. Liu, "Closed-loop iterative optimized fractional-order pid current control of pmsm," *IEEE Transactions on Industrial Informatics*, vol. 21, no. 2, pp. 1120–1129, 2025, DOI: 10.1109/TII.2024.3459962.

[15] Y. Belkhier, S. Fredj, H. Rashid, and M. Benbouzid, "Robust nonlinear control of permanent magnet synchronous motor drives: An evolutionary algorithm optimized passivity-based control approach with a high-order sliding mode observer," *Engineering Applications of Artificial Intelligence*, vol. 145, p. 110256, 2025, DOI: 10.1016/j.engappai.2025.110256.

[16] K. Shao, "A finite-time speed control method for permanent magnet synchronous motor drives based on sliding mode control and estimation theory," *Electrical Engineering*, vol. 107, no. 8, pp. 9795–9806, Aug 2025, DOI: 10.1007/s00202-025-03001-1.

[17] F. Beltran-Carbajal, A. Favela-Contreras, J. L. Hernandez-Avila, O. Olvera-Tapia, D. Sotelo, and C. Sotelo, "Dynamic output feedback control for desired motion tracking on synchronous motors," *International Transactions on Electrical Energy Systems*, vol. 30, no. 3, pp. 1–18, 2020, DOI: 10.1002/2050-7038.12260.

[18] A. Valderrabano-Gonzalez and C. E. Castañeda, "Enhanced ai-driven harmonic optimization in 36-pulses converters for scada integration," *Electronics*, vol. 14, no. 18, p. 3623, 2025, DOI: 10.3390/electronics14183623.

[19] F. Beltran-Carbajal, R. Tapia-Olvera, A. Valderrabano-Gonzalez, and I. Lopez-Garcia, "Adaptive neuronal induction motor control with an 84-pulse voltage source converter," *Asian Journal of Control*, vol. 23, no. 4, pp. 1603–1616, 2021, DOI: 10.1002/asjc.2322.

[20] A. Valderrabano and J. M. Ramirez, "A novel voltage source converter behind the statcom," *Electric Power Components and Systems*, vol. 38, no. 10, pp. 1161–1174, 2010, DOI: 10.1080/15325001003652918.

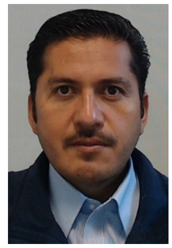

**Ruben Tapia-Olvera** obtained his BS in Electrical Engineering from Instituto Tecnológico de Pachuca, México in 1999; M.Sc. and Ph. D. in Electrical Engineering from CINVESTAV Guadalajara, México in 2002 and 2006, respectively. Currently, he is working as a full-time Professor in the Department of Electrical Energy at Universidad Nacional Autónoma de México, UNAM. His primary area of interest is in the modeling and control of electric machines and power systems with computational intelligence techniques.

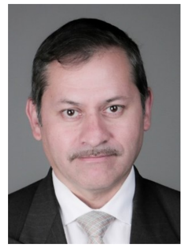

**Antonio Valderrabano-Gonzalez** received the B.S. in Industrial Electronics from the Instituto Tecnológico de Puebla (México), the M.Sc. degree in Electronics from the Instituto Nacional de Astrofísica, Óptica y Electrónica (México), and the Ph.D. in Electrical Engineering from Cinvestav Guadalajara (México); he is currently working as Professor at Universidad Panamericana Campus Guadalajara México. His research interests are Power Electronics, Control of Power Electronic Converters, FACTS devices, and Power Quality.

**Francisco Beltran-Carbajal** received the B.S. in Electromechanical Engineering from the Instituto Tecnológico de Zacatepec (México) and his Ph.D. in Electrical Engineering (Mechatronics) from the Centro de Investigación y Estudios Avanzados del Instituto Politécnico Nacional (CINVESTAV-IPN) in Mexico City. He is currently a Titular Professor in the Energy Department at Universidad Autónoma Metropolitana (UAM), Unidad Azcapotzalco in Mexico City. His main research interests are vibration control, system identification, rotating machinery, mechatronics, and automatic control of energy conversion systems.